Journal of Ceramic Processing Research. Vol. 21, No. 3, pp. 338~342 (2020)
(Received 16 February 2020, Received in revised form 18 March 2020, Accepted 20 March 2020)
https://doi.org/10.36410/jcpr.2020.21.3.338

J O U R N A L O F
Ceramic Processing Research

Effects of V_2O_5 on sinterability and microwave dielectric properties of $NaCa_4V_5O_{17}$ ceramics

Guoguang Yao*, Yang Li, Jingjing Tan, Cuijin Pei, Yan Zhang and Jia Chen
School of Science, Xi'an University of Posts and Telecommunications, Xi'an 710121, China

The $NaCa_4V_5O_{17}$ ceramics owing low sintering temperature had been prepared via conventional solid state reaction method using V_2O_5 as vanadium source. The sinterability, microwave dielectric characterisations and compatibility with Ag were investigated. Pure phase $NaCa_4V_5O_{17}$ with triclinic structure was confirmed by Rietveld refinement and Raman spectrum. The permittivity (ε_r) and quality factor (Qxf) values mainly depended on the relative density, whereas the temperature coefficient of resonant frequency (τ_f) value was closely connected with the tetrahedral distortion of $V_{(1)}O_4$. The $NaCa_4V_5O_{17}$ ceramics sintered at 800 °C owned high densification and moderate microwave dielectric performances under 10.7 GHz: ε_r = 9.5, Q×f = 34,200 GHz, τ_f = -90.0 ppm/°C, but poor chemical compatibility with Ag paste.

Key words: Ceramics, microwave dielectric properties, $NaCa_4V_5O_{17}$, tetrahedral distortion.

Introduction

In the future 10 years, 5G wireless communications will become the dominant wireless protocol for applications like Artificial Intelligence and the Internet of Things [1]. The rapid evolution of 5G wireless communications gives rise to higher requirement of microwave dielectric ceramics [2]. To address the requirements of 5G wireless communications, the dielectric ceramics must satisfy following primary dielectric characteristics: low ε_r ($\varepsilon_r \leq 10$) to increase signal transmission velocity, near-zero τ_f to ensure thermal stabilization at different operating temperatures, and high Qxf or low dielectric loss to decrease the power dissipation [3, 4]. Meanwhile, low sintering temperatures should be ensured to meet low-temperature co-sintered ceramic technology, which can be used to reduce the size of electronic devices [5, 6]. Therefore, the dielectric materials with superior performances and inherent lower sintering temperature received prodigious attention.

Recently, vanadium host compounds are followed with interest once again since their low sintering temperature and superior dielectric performances. Lots of vanadium-basic ceramics have been investigated for LTCC substrate applications, for example $Ca_5Co_4(VO_4)_6$, $(CaBi)(MoV)O_4$, $LiMgVO_4$, $(Bi, Ce)VO_4$, etc [7-11]. Quite recently, a novel $NaCa_4V_5O_{17}$ compounds with triclinic structure had been fabricated by Xie et al. [12]. Later, Fang et al. [13] first presented the microwave dielectric performances (e_r = 9.72, Q×f = 51,000 GHz, τ_f = -84 ppm/°C) of $NaCa_4V_5O_{17}$ ceramics. Considering the microwave dielectric performances of the ceramics are strongly depended on the craft parameters, including primary materials, ball milling and sintering conditions etc. [14]. The variation in one or more these parameters greatly influence the dielectric properties of such ceramics [15]. However, there is no related microwave dielectric properties study about $NaCa_4V_5O_{17}$ ceramics using V_2O_5 as vanadium source. Here, we reported the effects V_2O_5, as the vanadium source, on sinterability, microstructure, microwave dielectric performances as well as compatibility with silver of $NaCa_4V_5O_{17}$ ceramics.

Experimental

We fabricated $NaCa_4V_5O_{17}$ samples through the traditional solid-state route. V_2O_5 (99%), Na_2CO_3 (99.8%) and $CaCO_3$ (99%) were weighed according to stoichiometric $NaCa_4V_5O_{17}$, and then were ball milled for 8 h using alcohol and ZrO_2 balls for grinding media. The resultant milled powders were dried under 80 °C, followed by presintered under 600 °C/4 h, and then regrinded for further 8 h. The above presintered powders were mixed with 5wt % PVA, granulated and sieved through a No. 80 sieve. The granules were pressed at 200 MPa into compacts (Φ10 mm×5 mm). These compacts were heated at 500 °C for 2 h to exclude PVA, and then fired in air ambient under 750-850 °C dwelling for 4 h.

The phase constitutions in sintered specimens had been studied by X-ray powder diffraction (XRD, Smartlab, Japan) and Raman spectra (Jobin Yvon, Longjumeau, France) equipped with He-Ne laser and an output of 30

*Corresponding author:
Tel : +86 29 88166089
Fax: +86 29 88166333
E-mail: yaoguoguang@xupt.edu.cn

mW. Rietveld refinement of XRD patterns was carried out with the GSAS program [16]. Microstructures of $NaCa_4V_5O_{17}$ ceramics were observed through a scanning electron microscope (SEM, Hitachi, Tokyo, Japan). Archimedes' principle was carried out to determine the bulk densities. The ε_r and Qxf values of samples were evaluated by resonant cavity method using Rohde & Schwarz ZVB20 vector network analyzer under about 10-12 GHz. The τ_f value of samples was calculated between 25 and 85 °C according to Reference [17].

Results and Discussion

Fig. 1 exhibits the refined fit of $NaCa_4V_5O_{17}$ sintered under diverse temperatures to their diffraction patterns. The Rietveld refined lattice parameters, reliability factors and $V_{(1)}O_4$ tetrahedral distortion for all specimens are enumerated in Table 1. As shown in Fig. 1, the calculated XRD profiles based on $NaCa_4V_5O_{17}$ structural model closely fitted those of experimental ones, indicating the $NaCa_4V_5O_{17}$ ceramics crystallized in a triclinic structure with P-1(2) space group. Pure phase $NaCa_4V_5O_{17}$ without an obvious secondary phase was obtained for all samples sintered in the range of 750-850 °C. Moreover, as seen in Table 1, the achieved reliability factors (Rp, Rwp) are less than 15, suggesting the refined results are credible. Meanwhile, no obvious changes of unit cell volume were observed under different sintering temperatures.

The Raman spectrum of $NaCa_4V_5O_{17}$ sample fired under 800 °C is displayed in Fig. 2. Three distinct regions of Raman modes can be distinguished. The

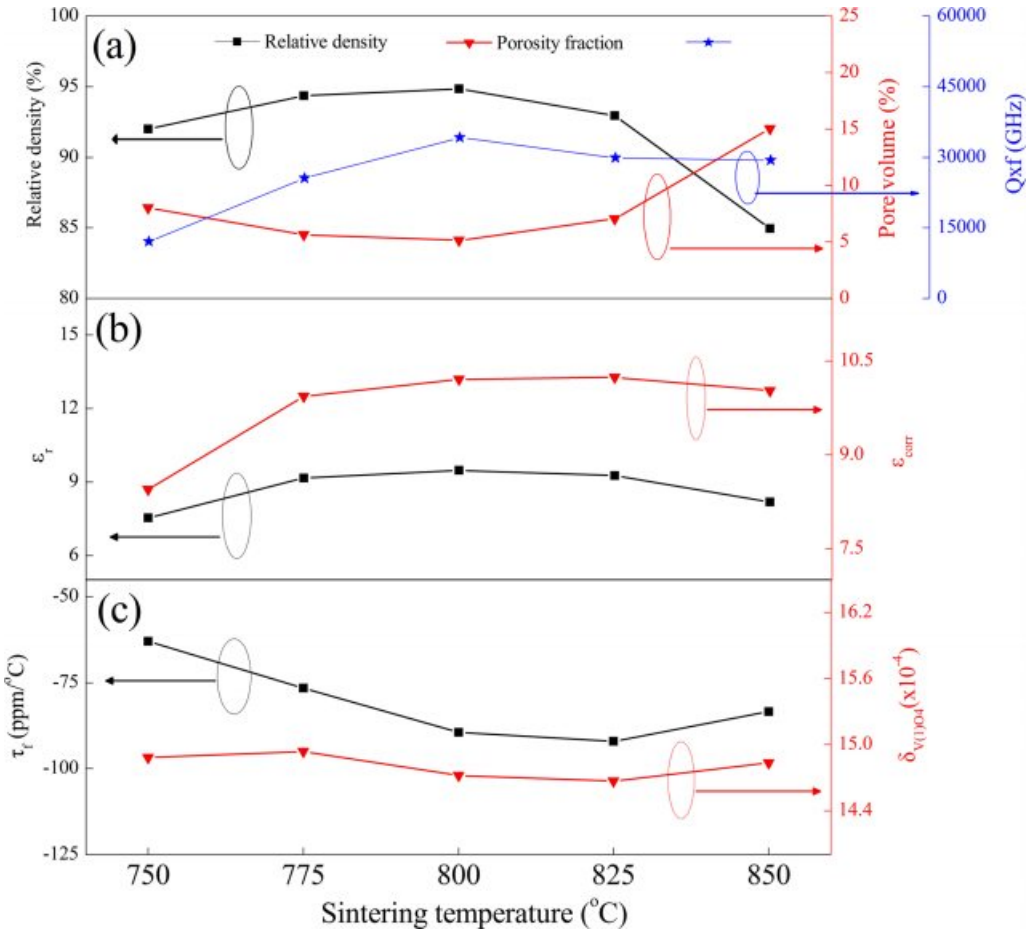

Fig. 1. Rietveld refinement patterns of $NaCa_4V_5O_{17}$ ceramics sintered at deferent temperatures.

Table 1. Rietveld refinement results and $V_{(1)}O_4$ tetrahedral distortion ($\delta_{V(1)O4}$) of $NaCa_4V_5O_{17}$ ceramics sintered at various temperatures.

S.T. (°C)	Rp (%)	R_wp (%)	a (Å)	b (Å)	c (Å)	V (Å^3)	$\delta_{V(1)O4}$ (‰)
750	4.82	8.02	6.942336	6.947236	15.502208	742.594	1.488
775	3.89	5.42	6.935585	6.940961	15.491529	740.720	1.493
800	10.14	14.22	6.938138	6.953815	15.494852	742.324	1.472
825	9.17	12.48	6.941581	6.947512	15.496531	742.289	1.466
850	7.33	10.28	6.943361	6.948496	15.497396	742.550	1.483

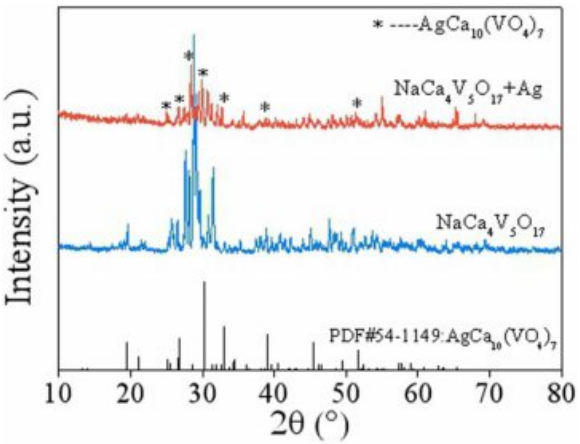

Fig. 2. Raman spectrum of $NaCa_4V_5O_{17}$ ceramics sintered at 800 °C.

first region located at 900-940 cm^{-1} is associated with terminal V-O (V = O) symmetric stretching vibrations [12]. The second region located at 550-880 cm^{-1} is related to the V-O-V antisymmetric or symmetric stretching vibrations [18]. The third region below the 400 cm^{-1} is ascribed to the peripheral modes [19].

Fig. 3 gives the typical SEM micrographs of $NaCa_4V_5O_{17}$ ceramics heated at distinct temperatures. From Figs. 3(a)-(c), the number of residual open pores was reduced accompanied by average grain size growth with an elevated temperature. And the 800 °C-sintered sample presented a relative compact and uniform microstructure with a mean grain size around 3.5 um, which is helpful to improve the dielectric properties of the $NaCa_4V_5O_{17}$ ceramics [20]. When the sintering temperature rose to 825 °C, excessive grain growth, uneven grain distribution and crack formed, these would deteriorate the dielectric performances of the present ceramics [21].

Fig. 4 presents the variations in relative density, pore volume, microwave dielectric properties and tetrahedral distortion of $NaCa_4V_5O_{17}$ ceramics heated at 750-850 °C. As shown in Fig. 4(a), the relative density was enhanced to the maximum (94.9%) under 800 °C and thereafter declined with an elevated temperature, which was agree with the above morphology analysis. In general, the Qxf value at microwave region of dielectric ceramics is predominated by extrinsic parameters like relative density, second phase and oxygen vacancies [22-24]. Considering the similar variation tendency between Qxf value and relative density of $NaCa_4V_5O_{17}$ ceramics, suggesting the Q×f value was predominated by the relative density. The ε_r is determined by density, dielectric polarizability and molecular volume [25, 26]. For a given compounds, its ε_r mainly depends on the relative density or porosity owing to the invariant dielectric polarizabilities and chemical formula [26]. Therefore, the changes of ε_r and ε_{corr} of $NaCa_4V_5O_{17}$ ceramics exhibited a tendency inverse or similar to the variation in porosity or relative density, and the corrected dielectric constant (ε_{corr}) was calculated according to reference [27]. It was reported that the τf value could

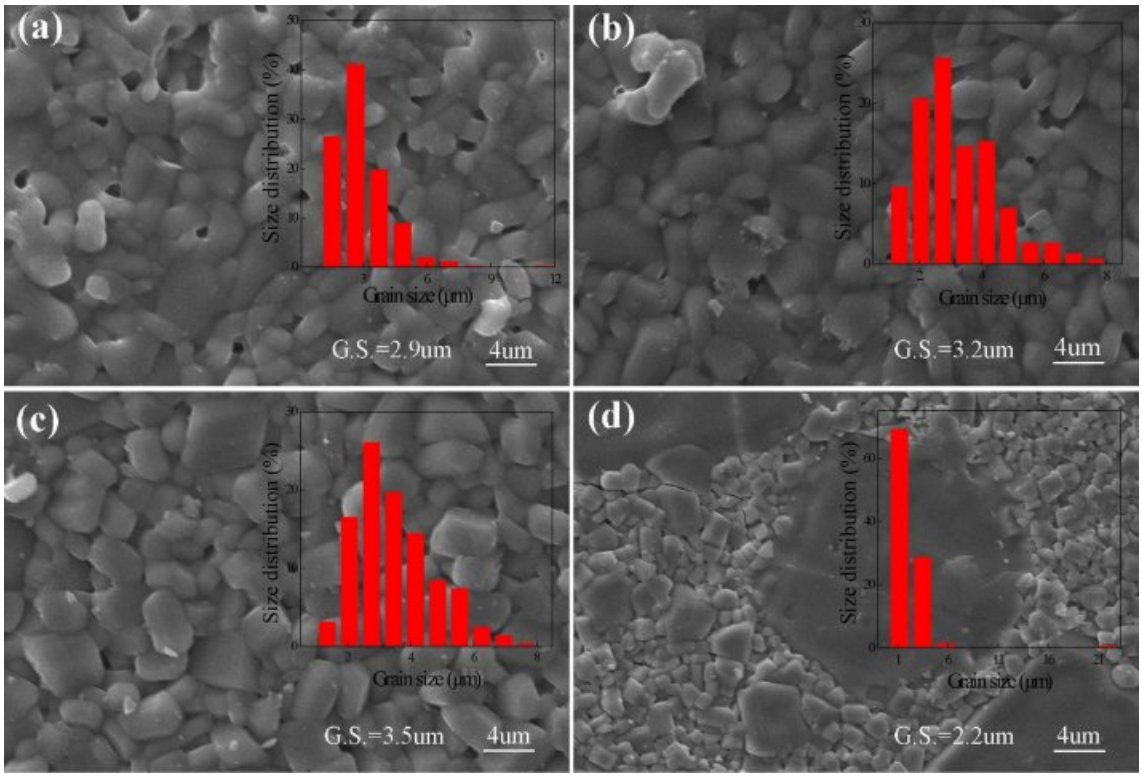

Fig. 3. SEM micrographs of $NaCa_4V_5O_{17}$ ceramics sintered at (a) 750 °C, (b) 775 °C, (c) 800 °C, (d) 825 °C.

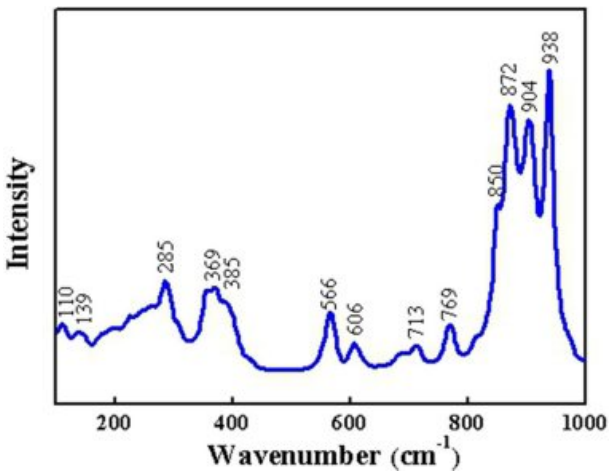

Fig. 4. Dependence of ρ_r, pore volume, ε_r, Qxf, τ_f and $\delta_{V(1)O4}$ on the firing temperature of $NaCa_4V_5O_{17}$ ceramics.

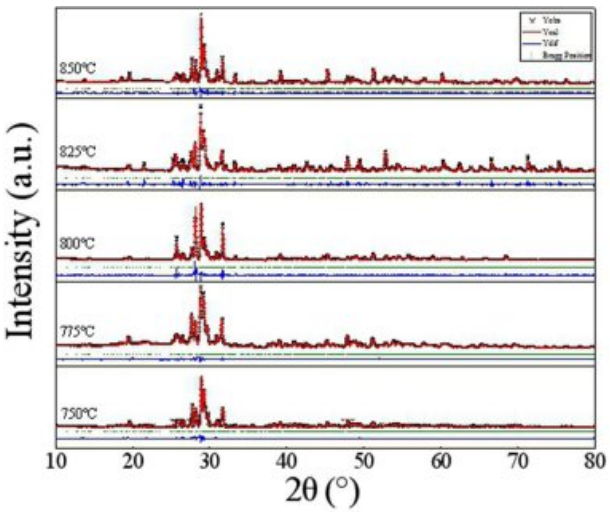

Fig. 5. XRD patterns of $NaCa_4V_5O_{17}$-20 wt% Ag mixture co-fired at 800 °C.

be determined by the distortion of oxygen polyhedral and phase composition [28, 29], which was also well represented in the present work. As seen in Fig. 4(c), the change of τ_f of $NaCa_4V_5O_{17}$ ceramics exhibited a tendency similar to that of the variation of $V_{(1)}O_4$ tetrahedral distortion ($\delta_{V(1)O4}$), indicating the τ_f is greatly affected by $\delta_{V(1)O4}$. The $\delta_{V(1)O4}$ calculated based the Rietveld refinement data and Shannon equation [30]. It is noted that the $NaCa_4V_5O_{17}$ ceramics in our cases possessed compatible ε_r (9.5) and τ_f (-90.0 ppm/°C) but inferior Qxf (34,200 GHz) value than that of $NaCa_4V_5O_{17}$ (ε_r = 9.72, τ_f = -84 ppm/°C, Qxf = 51,000 GHz) reported by Yin et al. [13], which may be due to the different vanadium source and processing conditions [31].

Fig. 5 depicts the XRD patterns of $NaCa_4V_5O_{17}$ presintered powder with 20 wt% Ag powder co-fired under 800 °C. As seen from Fig. 5, a new main phase $AgCa_{10}(VO_4)_7$ (JCPDS#54-1149) formed except for $NaCa_4V_5O_{17}$ phase, which was also not agree with the previous report [13]. This result showed that a chemical reaction between the basic phase $NaCa_4V_5O_{17}$ and Ag happened, which impeded its further application for LTCC.

Conclusions

The $NaCa_4V_5O_{17}$ ceramics owing low firing temperature had been prepared via the route of conventional solid state reaction. The impacts of V_2O_5 on the sinterability, microwave dielectric characterizations as well as chemical compatibility with Ag of present ceramics were investigated. The XRD and Raman spectrum revealed that the $NaCa_4V_5O_{17}$ ceramics crystallized in a triclinic structure with P-1(2) space group. The ε_r and Qxf values were dominated by the relative density, whereas the τ_f value was closely connected with the tetrahedral distortion of $V_{(1)}O_4$. Typically, the 800 °C-sintered $NaCa_4V_5O_{17}$ ceramics owned moderate microwave dielectric performances at measured frequency of 10.7 GHz: e_r = 9.5, Q×f = 34,200 GHz, τ_f = -90.0 ppm/°C, whereas its poor chemical compatibility with Ag paste affected its practical viability for LTCC applications.

Acknowledgements

This study was financially supported by China Post-doctoral Science Foundation (2015M582696), Shaanxi Province Postdoctoral Science Foundation, Education Department of Shaan xi Province (18JK0711), Science and technology plan project of Xi'an Bureau of Science and technology (GXYD17.19), and Innovation Funds of Graduate Programs of Xi'an Post and Telecommunications University (Grant Nos. CXJJLA2018008, CXJJLD2019020).

References

1. Q.B. Lin, K.X. Song, and B. Liu, Ceram. Int. 46 (2020) 1171-1177.
2. H. Li, C.Y. Cai, Q.Y. Xiang, B. Tang, J. Xiao, and S.R. Zhang, Ceram. Int. 45 (2019) 23157-23163.
3. J.J. Bian, X.Q. Sun, and Y.R. Xie, J. Eur. Ceram. Soc. 39 (2019) 4139-4143.
4. W.B. Hong, L. Li, H. Yan, and X.M. Chen, J. Am. Ceram. Soc. 102 (2019) 5934-5940.
5. X.H. Ma, S.H. Kweon, S. Nahm, C.Y. Kang, and Y.S. Kim, J. Eur. Ceram. Soc. 37 (2017) 605-610.
6. A. Pirvaram, E. Taheri-Nassaj, W.Z. Lu, and W. Lei, J. Am. Ceram. Soc. 102 (2019) 5213-5222.
7. R. Naveenraj, E.K. Suresh, and J. Dhanya, Eur. J. Inorg. Chem. 2019 (2019) 949-955.
8. H.H. Guo, D. Zhou, L.X. Pang, and Z.M. Qi, J. Eur. Ceram. Soc. 39 (2019) 2365-2373.
9. G.G. Yao, P. Liu, X.G. Zhao, J.P. Zhou, and H.W. Zhang, J. Eur. Ceram. Soc. 34 (2014) 2983-2987.
10. H.H. Guo, D. Zhou, and W.F. Liu, J. Am. Ceram. Soc. 103 (2019) 423-431.

11. G.G. Yao, X.S. Hu, P. Liu, and J.G. Xu, J. Mater. Sci: Mater. Electron. 26 (2015) 1795-1798.
12. Z.Q. Xie, S.C. Cheng, S.W. Li, and H.Q. Ding, J. Solid. State. Chem. 269 (2019) 94-99.
13. C.Z. Yin, C.C. Li, L. Fang et al., J. Eur. Ceram. Soc. 40 (2020) 386-390.
14. Y.C. Liou, S.L. Yang, and S.Y. Chu, J. Alloy. Compd. 576 (2013) 161-169.
15. C.J. Pei, C.D. Hou, Y. Li, G.G. Yao, P. Liu, and H.W. Zhang, J. Alloy. Compd. 792 (2019) 46-49.
16. A.C. Larson and R.B. Von Dreele, Los Alamos National Laboratory Report LAUR 86 (2004)
17. G.G. Yao, C.D. Hou, C.J. Pei, and P. Liu, Ferroelectrics. 536 (2018) 156-161.
18. A. Sharma, M. Varshney, and K.H. Chae, Rsc. Adv. 8 (2018) 26423-26431.
19. E.K. Suresh, K. Prasad, N.S. Arun, and R. Ratheesh, J. Electron. Mater. 45 (2016) 2996-3002.
20. S.P. Wu, D.F. Chen, C. Jiang, Y.X. Mei, and Q. Ma, Mater. Lett. 91 (2013) 239-241.
21. J.B. Song, K.X. Song, J.S. Wei, H.X. Lin, and J.M. Xu, J. Alloy. Compd. 731 (2018) 264-270.
22. J.M. Kim, H.W. Jo, and E.S. Kim, Int. J. Appl. Ceram. Technol. 16 (2019) 2053-2059.
23. R.C. Pullar, S.J. Penn, I.M. Reaney, and N.M. Alford, J. Eur. Ceram. Soc. 29 (2009) 419-424.
24. S.B An, J. Jiang, J.Z. Wang, L. Gan, and T.J. Zhang, Ceram. Int. 46 (2020) 3960-3967.
25. C.J. Pei, G.G. Yao, and Z.Y. Ren, J. Ceram. Process. Res. 17 (2016) 681-684.
26. Y. Wang L.W. Shi, and W.S. Xia, Ceram. Int. 46 (2020) 6984-6986.
27. T. Hanai and Z. Kolloid, Kolloid-Zeitschrift. 171 (1960) 23-30.
28. K.M. Manu, K.A. Lazar, R. Ubic, and M.T. Sebastian, J. Am. Ceram. Soc. 96 (2013) 1504-1511.
29. G.G. Yao, J. Ceram. Process. Res. 16 (2015) 4144.
30. W.H. Baur, Acta. Crystallogr. Sect. B. 30 (1974) 1195-1215.
31. M. Li, A. Feteira, M.T. Lanagan, and C.A. Randall, J. Am. Ceram. Soc. 93 (2010) 4087-4095.